

**Pacific  
Institute**  
for the Mathematical Sciences

<http://www.pims.math.ca>  
[pims@pims.math.ca](mailto:pims@pims.math.ca)

# Multifrequency inverse obstacle scattering: the point source method and generalized filtered backprojection

D. Russell Luke

Pacific Institute for the Mathematical Sciences  
Simon Fraser University  
Burnaby BC V5A 1S6  
Canada

Preprint number: PIMS-03-4  
Received on February 6, 2003

---

	<b>PIMS-Director</b>	<b>director@pims.math.ca</b>	<b>(604) 822-3922</b>		
<b>SFU-site</b>	<b>sfu@pims.math.ca</b>	<b>(604) 268-6655</b>		<b>UCalgary-site</b>	<b>uc@pims.math.ca</b> <b>(403) 220-3951</b>
<b>UAlberta-site</b>	<b>ua@pims.math.ca</b>	<b>(780) 492-4308</b>		<b>UVic-site</b>	<b>uvic@pims.math.ca</b> <b>(250) 472-4271</b>
<b>UBC-site</b>	<b>ubc@pims.math.ca</b>	<b>(604) 822-3922</b>		<b>UWashington-site</b>	<b>uw@pims.math.ca</b> <b>(206) 543-1173</b>



# Multifrequency inverse obstacle scattering: the point source method and generalized filtered backprojection

D. Russell Luke

*Pacific Institute for the Mathematical Sciences, Simon Fraser University,  
Burnaby, British Columbia V5A 1S6, Canada*

---

## Abstract

This work is a study of strategies for obstacle reconstruction from multifrequency far field scattering data. We outline two strategies for obstacle reconstruction from multifrequency far field scattering data: the point source method proposed by Potthast for solving inverse scattering problems with single frequency data in the resonance region, and filtered backprojection techniques based on the physical optics approximation for high frequency scattering. Our implementation of the point source method can be viewed as a generalized filtered backprojection algorithm, the key to which is the construction of the filter used in the backprojection operator. Numerical examples indicate that the critical factor for reconstructions in multifrequency settings is the frequency dependence of the filter.

*Key words:* inverse problems, scattering theory, image processing

---

## 1 Introduction

In recent years many innovative algorithms have appeared for inverse scattering applications in the resonance region. Of particular interest here is the point source method proposed by Potthast [14–16]. This and other algorithms of this type [3–5, 7] share the feature of splitting the original ill-posed nonlinear inverse problem into an ill-posed linear inverse problem, and a well-posed nonlinear problem. These algorithms were designed primarily with single-, low-frequency applications in mind. We compare the point source method to

---

*Email address:* `drluke@pims.math.ca` (D. Russell Luke).

a method based on a well known high-frequency technique that employs the classical physical optics approximation.

We begin with a brief orientation to forward scattering. Inverse scattering, including the point source method and physical optics approximations, is treated in Section 3. Numerical results are presented in Section 4.

## 2 Forward scattering

This discussion is limited to scattering of small-amplitude, monochromatic, time-harmonic waves from an impenetrable, sound-soft obstacle embedded in an isotropic homogeneous medium. The obstacle is identified by its support  $\Omega \subset \mathbb{R}^m$ ,  $m = 2$  or  $3$ . Throughout this work, unless otherwise stated,  $\Omega$  is assumed to be a bounded domain with connected  $C^2$  (twice continuously differentiable) boundary  $\partial\Omega$  and the unit outward normal  $\nu$ . The governing equation for this setting is the Helmholtz equation:

$$[\Delta + \kappa^2]v(x, \kappa) = 0, \quad x \in \overline{\Omega}^\circ \subset \mathbb{R}^m, \quad (1)$$

where  $\Delta$  denotes the Laplacian,  $\kappa \geq 0$  is the *frequency* or *wavenumber* and  $\overline{\Omega}^\circ := \mathbb{R}^m \setminus \overline{\Omega}$ . Solutions to Eq.(1) are complex-valued scalar waves parameterized by  $\kappa$ ,  $v : \overline{\Omega}^\circ \times \mathbb{R}_+ \rightarrow \mathbb{C}$ . The surface of the obstacle is assumed to be perfectly absorbing or *sound-soft*. This is modeled with Dirichlet boundary conditions:  $v = f$  on  $\partial\Omega$  where,  $f$  is continuous on  $\partial\Omega$ .

Consider an *incident field*  $v^i : \mathbb{R}^m \times \mathbb{R}_+ \rightarrow \mathbb{C}$  that, for fixed  $\kappa$ , is an *entire solution* to the Helmholtz equation on  $\mathbb{R}^m$ , that is  $v^i$  satisfies Eq.(1) on  $\mathbb{R}^m$ . The *scattering problem* is to find the *total field*  $v : \Omega^\circ \times \mathbb{R}_+ \rightarrow \mathbb{C}$  that satisfies Eq.(1) on  $\overline{\Omega}^\circ$  and  $v = v^i + v^s$  where  $f = 0$  for the boundary condition, and where  $v^s : \Omega^\circ \times \mathbb{R}_+ \rightarrow \mathbb{C}$  is the *scattered field* satisfying Eq.(1) on  $\overline{\Omega}^\circ$  and the *Sommerfeld Radiation Condition*:

$$r^{\frac{m-1}{2}} \left( \frac{\partial}{\partial r} - i\kappa \right) v^s(x, \kappa) \rightarrow 0, \quad r = |x| \rightarrow \infty, \quad (2)$$

uniformly in all directions. The scattering problem has a unique solution [3]. At large distances from the obstacle  $\Omega$ , the scattered field  $v^s$  is characterized by the *far field pattern*  $v^\infty : \mathbb{S} \times \mathbb{R}_+ \rightarrow \mathbb{C}$  on the set of directions  $\mathbb{S} := \{x \in \mathbb{R}^m \mid |x| = 1\}$ . We denote the direction of a vector  $x \in \mathbb{R}^m$  by  $\hat{x} := \frac{x}{|x|}$ .

For fixed  $\kappa > 0$ , let  $v^s(\cdot, \kappa) \in C^2(\overline{\Omega}^\circ) \cap C(\Omega^\circ)$  satisfy Eq.(1) and Eq.(2) with Dirichlet boundary conditions. Denote the free-space fundamental solution to Eq.(1) by  $\Phi : \mathbb{R}^m \times \mathbb{R}^m \times \mathbb{R}_+ \rightarrow \mathbb{C}$  (see [Eq.(3.60) and Eq.(2.1)] [3]). Then  $v^s$  satisfies Green's formula [3, Eq.2.5], also known as the Integral Theorem of

Kirchhoff and Helmholtz, for  $x \in \overline{\Omega}^\circ$  and  $\kappa > 0$  Let  $v$  be the corresponding solution to the scattering problem for a sound-soft scatterer (i.e.  $v = 0$  on  $\partial\Omega$ ) with entire incident wave  $v^i$ . Then  $v(x, \kappa) = v^i(x, \kappa) + v^s(x, \kappa)$ ,  $x \in \overline{\Omega}^\circ, \kappa > 0$ , and Green's formula applied to  $v^s$ , together with the application of Green's Theorem applied to  $v^i$  and  $\Phi$ , yield the following formalization of Huygens's principle [3, Thm. 3.12]

$$v^s(x, \kappa) = - \int_{\partial\Omega} \frac{\partial v(z, \kappa)}{\partial \nu(z)} \Phi(x, z, \kappa) ds(z), \quad x \in \overline{\Omega}^\circ, \kappa > 0. \quad (3)$$

The corresponding far-field pattern is given by

$$v^\infty(\hat{x}, \kappa) = -\beta(\kappa) \int_{\partial\Omega} \frac{\partial v(z, \kappa)}{\partial \nu(z)} e^{-i\kappa \hat{x} \cdot z} ds(z), \quad \hat{x} \in \mathbb{S}. \quad (4)$$

where  $\beta(\kappa)$  is given by [3, Eq.(2.13) and Eq.(3.64)]

$$\beta(\kappa) = \frac{e^{-i\frac{\pi}{4}}}{\sqrt{8\pi\kappa}}, \quad \text{for } m = 2 \quad \text{and} \quad \beta(\kappa) = \frac{1}{4\pi}, \quad \text{for } m = 3. \quad (5)$$

We reserve special notation for incident *plane waves* denoted by

$$u^i(x, \hat{\eta}, \kappa) := e^{i\kappa x \cdot \hat{\eta}}, \quad x \in \mathbb{R}^m, \hat{\eta} \in \mathbb{S}, \kappa \in \mathbb{R}_+. \quad (6)$$

Here  $\hat{\eta} \in \mathbb{S}$ , indicates the *direction of incidence*.

### 3 Inverse scattering

Let  $\Gamma \subset \mathbb{S}$  denote an open set of directions on  $\mathbb{S}$ . Here,  $\Gamma$  models the aperture on which our sensors lie. In our numerical experiments, this is a symmetric interval of the unit sphere centered with respect to the direction of the incident field. The far field  $u^\infty$  due to an incident plane wave with direction  $\hat{\eta} \in \mathbb{S}$  is measured at points  $\hat{y} \in \Gamma$ . Define the operator  $\widetilde{H}_\kappa : L^2(-\Gamma) \rightarrow L^\infty(\mathbb{R}^m)$  by

$$(\widetilde{H}_\kappa g)(x) := \int_{\Gamma} e^{i\kappa x \cdot (-\hat{y})} g(-\hat{y}) ds(\hat{y}), \quad x \in \mathbb{R}^m, g \in L^2(-\Gamma). \quad (7)$$

The corresponding family of functions parameterized by  $\kappa$  and mapping  $\mathbb{R}^m$  to  $\mathbb{C}$ ,  $\widetilde{h}_g(\cdot, \kappa) := (\widetilde{H}_\kappa g)(\cdot)$ , consists of entire solutions to the Helmholtz equation for fixed  $\kappa$ . Note that the function  $g$  is only defined on  $-\Gamma$  where  $-\Gamma$  is the mirror image of the interval  $\Gamma$  on the unit sphere:  $\hat{y} \in \Gamma \iff -\hat{y} \in -\Gamma$ . When the aperture is the entire sphere,  $\Gamma = \mathbb{S}$ , then we denote the corresponding function, also known as the Herglotz wave function [3, pp.55], by  $h_g(\cdot, \kappa)$ . In contrast to the density  $g$  for limited apertures, the far field due to

scattering from an incident plane wave  $u^\infty$  is defined on  $\Gamma$  with any incident wave direction  $\hat{\eta}$ . The region  $\Gamma$  defines a *virtual* aperture corresponding to the physical aperture  $\Gamma$  on which the sensors lie. Looking ahead to filtered backprojection, the virtual aperture in the case of scattering is analogous to the actual measurement array in x-ray transmission tomography. For example, in classical parallel scanning x-ray tomography, a source with direction  $-\hat{\eta}$  emitted from the point  $\hat{\eta} \in \Gamma$  has a corresponding receiver located at the point  $-\hat{\eta} \in -\Gamma$ .

### 3.1 The Point Source Method

The next theorem establishes the central principle behind the point source method. Here the duality of incident point sources and incident plane waves is used to construct a backprojection operator mapping the far field due to an incident plane wave to the corresponding scattered field at an arbitrary point  $z$  in the near field. In fact, we construct a *family* of backprojection operators with kernel  $g(\cdot, z, \kappa)$  depending on the location  $z$  and wavenumber  $\kappa$  of the field to be reconstructed,  $\mathcal{A}_g : L^2(\Gamma \times \mathbb{S} \times \mathbb{R}_+) \rightarrow L^2(\mathbb{R}^m \times \mathbb{S} \times \mathbb{R}_+)$ , defined by

$$(\mathcal{A}_g \psi)(z, \hat{\eta}, \kappa) := \int_{\Gamma} \psi(\hat{y}, \hat{\eta}, \kappa) \frac{g(-\hat{y}, z, \kappa)}{\beta(\kappa)} ds(\hat{y}), \quad \psi \in L^2(\Gamma \times \mathbb{S} \times \mathbb{R}_+), \quad (8)$$

for  $\beta(\kappa)$  given by Eq.(5). The construction of such a backprojection operator relies on the approximation of the fundamental solution  $\Phi$  at frequency  $\kappa$  due to a point source at the point  $z$  by the function

$$\tilde{h}_g(x, z, \kappa) := (\tilde{H}_\kappa g(-\hat{y}, z, \kappa))(x) = \int_{\Gamma} e^{i\kappa x \cdot (-\hat{y})} g(-\hat{y}, z, \kappa) ds(\hat{y}), \quad (9)$$

for  $x \in \mathbb{R}^m$ ,  $g(\cdot, z, \kappa) \in L^2(-\Gamma)$ . The arguments in  $g(\cdot, z, \kappa)$  explicitly denote the dependence of the density on the location and frequency of the point source. Surely we cannot hope to approximate  $\Phi$  *everywhere*, but it can be shown that if we choose the density  $g(\cdot, z, \kappa)$  such that  $\tilde{h}_g(\cdot, z, \kappa)$  approximates  $\Phi(\cdot, z, \kappa)$  on the  $C^2$  boundary of a bounded, connected domain  $\Omega_a$  satisfying  $\bar{\Omega} \subset \Omega_a$ , then  $\mathcal{A}_g$  with kernel  $g(\cdot, z, \kappa)$  operating on  $u^\infty(\hat{y}, \hat{\eta}, \kappa)$  will approximate the scattered field  $u^s(z, \hat{\eta}, \kappa)$ . The theorem below is a restatement of [11, Theorem 2.1], which includes the limited aperture setting; the original idea in the full aperture setting is due to Potthast and can be found in [14, 16].

**Theorem 1 (Backprojection)** *Let  $\Omega_a \subset \mathbb{R}^m$  be a bounded domain (the domain of approximation) with connected  $C^2$  boundary such that  $\bar{\Omega} \subset \Omega_a$ . For the fixed wavenumber  $\kappa > 0$ , assume that  $\kappa^2$  is not a Dirichlet eigenvalue of the negative Laplacian on the interior of  $\Omega_a$ . Denote the fundamental solution to Eq.(1) with singularity at  $z \in \mathbb{R}^m \setminus \bar{\Omega}_a$  by  $\Phi(\cdot, z, \kappa)$ , and let the function*

$\tilde{h}_g(\cdot, z, \kappa) : \mathbb{R}^m \rightarrow \mathbb{C}$  be defined by Eq.(9). Given any  $\epsilon > 0$ , there exists a constant  $c > 0$  such that, for all  $g(\cdot, z, \kappa) \in L^2(-\Gamma)$  satisfying

$$\left\| \Phi(\cdot, z, \kappa) - \tilde{h}_g(\cdot, z, \kappa) \right\|_{C(\partial\Omega_a)} \leq \epsilon, \quad (10)$$

the following holds:

$$\left| u^s(z, \hat{\eta}, \kappa) - (\mathcal{A}_g u^\infty)(z, \hat{\eta}, \kappa) \right| < c\epsilon, \quad (11)$$

where  $u^s$  and  $u^\infty$  are the scattered field and far field pattern due to an incident plane wave with direction  $\hat{\eta} \in \mathbb{S}$  and  $\mathcal{A}_g$  is defined by Eq.(8).

For an incident plane wave of fixed direction  $\hat{\eta}$ , the point source method involves constructing a density  $g$  at every point  $z \in \mathbb{R}^m \setminus \bar{\Omega}_a$  to satisfy Eq.(10) and using this density to construct the backprojection operator  $\mathcal{A}_g$  approximating the scattered field  $u^s$  at the point  $z$  via Eq.(11). There are many possibilities for calculating  $g$  depending on the size of the parameter  $\epsilon$  in Eq.(10) and the choice of the domain of approximation  $\Omega_a$ . The approximating domain need not – indeed *will not* – be the same for every point  $z$ . Neither will the condition  $\Omega \subset \Omega_a$  be satisfied for every domain of approximation since the precise location and size of the object  $\Omega$  is not known. In Section 3.2 we derive rough estimates for  $g$  based on high-frequency physical-optics approximations. Before discussing this technique, we review an optimization approach for calculating  $g$  originally proposed by Potthast [14, 16] for the case of full aperture scattering.

The density we select, denoted  $g_*(\cdot, z, \kappa)$ , is the one that, for a fixed frequency  $\kappa$  and fixed point  $z$ , solves a regularized least squares minimization problem. Recall that when  $\Gamma = \mathbb{S}$  we write  $h_g = \tilde{h}_g$  for  $\tilde{h}_g$  defined by Eq.(9). The restriction to a limited aperture  $\Gamma \subset \mathbb{S}$  is treated as a penalty in the objective of the following optimization problem

$$\begin{aligned} \text{minimize } & \left\| \Phi(\cdot, z, \kappa) - h_g(\cdot, z, \kappa) \right\|_{L^2(\partial\Omega_a)}^2 + \alpha \left\| g(\cdot, z, \kappa) \right\|_{L^2(\mathbb{S})}^2 \\ & + \tilde{\alpha} \left\| (1 - \mathcal{X}_{-\Gamma})g(\cdot, z, \kappa) \right\|_{L^2(\mathbb{S})}^2 \end{aligned} \quad (12)$$

over  $g(\cdot, z, \kappa) \in L^2(\mathbb{S})$  where  $\mathcal{X}_{-\Gamma}$  is the indicator function for the reflected aperture  $-\Gamma$ , that is  $\mathcal{X}_{-\Gamma}(\hat{y}) = 1$  for  $\hat{y} \in -\Gamma$  and  $\mathcal{X}_{-\Gamma}(\hat{y}) = 0$  otherwise.

The first challenge is to choose the appropriate domain of approximation  $\Omega_a$  and regularization parameters  $\alpha$  and  $\tilde{\alpha}$  without knowing exactly where or how large the obstacle is. To do this we create a generating domain  $\Omega_0$  for a point source located at  $z = 0$ , and then calculate the corresponding density  $g_*(\cdot, 0, \kappa)$

satisfying Eq.(12). The spatial invariance of the fundamental solution allows one to *scan* the computational domain by translations of  $\Omega_0$ . The density  $g_*(\cdot, z, \kappa)$  corresponding to the translated generating domain can be written explicitly in terms of  $g_*(\cdot, 0, \kappa)$  as the next proposition shows.

**Proposition 2** *Let  $\Omega_0$  be any bounded test domain in  $\mathbb{R}^m \setminus \{0\}$  with connected  $C^2$  boundary and for which  $\kappa$  is not an eigenvalue for the interior Dirichlet problem. Consider the problem*

$$\begin{aligned} \text{minimize } & \left\| \Phi(\cdot, 0, \kappa) - h_g(\cdot, 0, \kappa) \right\|_{L^2(\partial\Omega_0)}^2 + \alpha_0 \left\| g(\cdot, 0, \kappa) \right\|_{L^2(\mathbb{S})}^2 \\ & + \tilde{\alpha}_0 \left\| (1 - \mathcal{X}_{-\Gamma})g(\cdot, 0, \kappa) \right\|_{L^2(\mathbb{S})}^2 \end{aligned} \quad (13)$$

over  $g(\cdot, 0, \kappa) \in L^2(\mathbb{S})$  where the function  $h_g$  is the extension to  $\mathbb{S}$  of  $\tilde{h}_g$  defined by Eq.(9). This problem has a unique solution  $g_*(\cdot, 0, \kappa)$ . Moreover, the optimal solution to the problem

$$\begin{aligned} \text{minimize } & \left\| \Phi(\cdot, z, \kappa) - h_g(\cdot, z, \kappa) \right\|_{L^2(\partial(\Omega_0+z))}^2 + \alpha_0 \left\| g(\cdot, z, \kappa) \right\|_{L^2(\mathbb{S})}^2 \\ & + \tilde{\alpha}_0 \left\| (1 - \mathcal{X}_{-\Gamma})g(\cdot, z, \kappa) \right\|_{L^2(\mathbb{S})}^2 \end{aligned} \quad (14)$$

over  $g(\cdot, z, \kappa) \in L^2(\mathbb{S})$  is given by

$$g_*(\hat{y}, z, \kappa) = e^{-i\kappa z \cdot \hat{y}} g_*(\hat{y}, 0, \kappa), \quad \hat{y} \in \mathbb{S}. \quad (15)$$

*Proof.* The linearity of the operator  $\widetilde{H}_\kappa$  with respect to  $g(\cdot, 0, \kappa)$  and the fact that the  $L^2$  norm squared is convex yield uniqueness for the optimization problem Eq.(13). Existence follows from the fact that the space  $L^2(\mathbb{S})$  is closed.

To prove the second statement, note that the norms on the space  $L^2(\mathbb{S})$  are invariant under multiplication by the complex factor  $e^{-i\kappa z \cdot \hat{y}}$ ; so one need only show that

$$\left\| \Phi(\cdot, 0, \kappa) - h_*(\cdot, 0, \kappa) \right\|_{L^2(\partial(\Omega_0))}^2 = \left\| \Phi(\cdot, z, \kappa) - h_*(\cdot, z, \kappa) \right\|_{L^2(\partial(\Omega_0+z))}^2,$$

where  $h_*(\cdot, 0, \kappa)$  denotes the Herglotz wave function with kernel  $g_*(\cdot, 0, \kappa)$ , a solution to Eq.(13), and where  $g_*(\cdot, z, \kappa)$  is given by Eq.(15). To see this, define  $h_*'(x, z, \kappa)$  by

$$h_*'(x, z, \kappa) := \int_{\mathbb{S}} e^{i\kappa x \cdot (-\hat{y})} g_*'(-\hat{y}, z, \kappa) ds(\hat{y})$$



where  $g'_*(-\hat{y}, z, \kappa) = e^{i\kappa z \cdot (-\hat{y})} g_*(-\hat{y}, z, \kappa)$ . Note that  $h_*(x, z, \kappa) = h'_*(x - z, z, \kappa)$ . By the spatial invariance of the fundamental solution,  $\Phi(x, z, \kappa) = \Phi(x - z, 0, \kappa)$ , which yields

$$\begin{aligned} \left\| \Phi(\cdot, z, \kappa) - h_*(\cdot, z, \kappa) \right\|_{L^2(\partial(\Omega_0+z))}^2 &= \left\| \Phi(\cdot - z, 0, \kappa) - h'_*(\cdot - z, z, \kappa) \right\|_{L^2(\partial(\Omega_0+z))}^2 \\ &= \left\| \Phi(\cdot, 0, \kappa) - h'_*(\cdot, z, \kappa) \right\|_{L^2(\partial(\Omega_0))}^2 \\ &\geq \left\| \Phi(\cdot, 0, \kappa) - h_*(\cdot, 0, \kappa) \right\|_{L^2(\partial(\Omega_0))}^2. \end{aligned} \quad (16)$$

Now, since  $g_*(\hat{y}, 0, \kappa)$  is the optimal solution to Eq.(13), equality holds in Eq.(16) if  $h'_*(x, z, \kappa) = h_*(x, 0, \kappa)$ , that is, if

$$g'_*(\hat{y}, z, \kappa) = e^{i\kappa z \cdot \hat{y}} g_*(\hat{y}, z, \kappa) = g_*(\hat{y}, 0, \kappa).$$

□

As a consequence of Theorem 2 one need solve the optimization problem Eq.(12) once for the generating domain of approximation  $\Omega_0$ . The solution to Eq.(13) can be written explicitly as the solution to the normal equations. For details see [11, 14, 16]. The backprojection operator given by Eq.(8) corresponding to these translated domains can be written in terms of the generating density  $g_*(\cdot, 0, \kappa)$  as

$$\begin{aligned} (\tilde{\mathcal{A}}_{g_*} u^\infty)(z, \hat{\eta}, \kappa) &:= \\ \int_{\Gamma} u^\infty(\hat{x}, \hat{\eta}, \kappa) \frac{g_*(-\hat{x}, 0, \kappa)}{\beta(\kappa)} e^{-i\kappa z \cdot (-\hat{x})} ds(\hat{x}), \quad z \in \mathbb{R}^m. \end{aligned} \quad (17)$$

The points  $z$  satisfying the hypotheses of Theorem 1 depend on the geometry of this generating domain and that of the scatterer  $\Omega$ . Where the hypotheses are not satisfied, the behavior of the function represented in Eq.(17) is in general unpredictable, though it is often observed that the pointwise values are large [11, 12, 14, 16]. The domain of approximation that we use is shown in Figure 1(a). This domain is chosen in particular to allow us to exploit the radial symmetry of point sources.

### 3.2 Physical optics and filtered backprojection

The high frequency asymptotics of the far-field pattern yield a variety of shape reconstruction techniques. In this section we briefly review the well-known

Fourier inversion method for reconstructing sound-soft scatterers based on the classical *physical optics* or *Kirchhoff* approximation. Our description is terse. The usual justification for Fourier inversion is limited to *convex* obstacles [2], however, with some further assumptions on the regularity of  $\Omega$ , this can be extended to weakly nonconvex obstacles [1, 9].

To begin, let  $u^i(\cdot, \hat{\eta}, \kappa)$  be an incident plane wave with direction  $\hat{\eta}$ . Define  $\partial\Omega_+$  to be the illuminated side of the scattering domain  
 $\partial\Omega_+ := \{x \in \partial\Omega \mid \nu(x) \cdot \hat{\eta} < 0\}$ . The shadow of the scattering domain,  $\partial\Omega_-$ , is defined as  $\partial\Omega_- := \partial\Omega \setminus \overline{\partial\Omega_+}$ . The physical optics or Kirchhoff approximation is written

$$\frac{\partial u^s(x, \hat{\eta}, \kappa)}{\partial \nu(x)} \approx \begin{cases} \frac{\partial u^i(x, \hat{\eta}, \kappa)}{\partial \nu(x)}, & x \in \partial\Omega_+ \\ -\frac{\partial u^i(x, \hat{\eta}, \kappa)}{\partial \nu(x)}, & x \in \partial\Omega_- \end{cases}, \quad \kappa \gg 0. \quad (18)$$

In words, for large  $\kappa$  (that is, small wavelengths), the obstacle can be locally approximated by a plane, and the scattered field behaves accordingly. Substituting Eq.(18) into Eq.(3) yields the identity

$$u^s(x, \hat{\eta}, \kappa) \approx -2 \int_{\partial\Omega_+} \frac{\partial u^i(z, \hat{\eta}, \kappa)}{\partial \nu(z)} \Phi(x, z, \kappa) ds(z), \quad \kappa \gg 0. \quad (19)$$

The corresponding far field pattern thus has the following asymptotic behavior with respect to the wavenumber:

$$u^\infty(\hat{x}, \hat{\eta}, \kappa) \approx -2\beta(\kappa) \int_{\partial\Omega_+} \frac{\partial u^i(z, \hat{\eta}, \kappa)}{\partial \nu(z)} e^{-i\kappa \hat{x} \cdot z} ds(z), \quad (20)$$

for  $\hat{x}, \hat{\eta} \in \mathbb{S}$  and  $\kappa(\hat{x} - \hat{\eta}) \gg 0$ . Similarly, on the shadow of  $\Omega$  we have

$$u^\infty(\hat{x}, -\hat{\eta}, \kappa) \approx 2\beta(\kappa) \int_{\partial\Omega_-} \frac{\partial u^i(z, -\hat{\eta}, \kappa)}{\partial \nu(z)} e^{-i\kappa \hat{x} \cdot z} ds(z). \quad (21)$$

Let  $\widehat{\mathcal{X}}_\Omega$  denote the Fourier transform of the indicator function of the obstacle  $\Omega$ :

$$\widehat{\mathcal{X}}_\Omega(\xi) := \frac{1}{(2\pi)^{m/2}} \int_{\mathbb{R}^m} \mathcal{X}(z) e^{-i\xi \cdot z} dz,$$

with  $\mathcal{X}_\Omega(z)$  the indicator function of the scatterer  $\Omega$ . Then Green's *first* theorem [3, Equation (2.2)], together with Eq.(20) and Eq.(21) for  $\kappa(\hat{x} - \hat{\eta}) \gg 0$ , yield

$$u^\infty(\hat{x}, \hat{\eta}, \kappa) + \overline{u^\infty(-\hat{x}, -\hat{\eta}, \kappa)} \quad (22)$$

$$\begin{aligned} &\approx -2\beta(\kappa) \int_{\partial\Omega} \frac{\partial u^i(z, -\hat{\eta}, \kappa)}{\partial \nu(z)} e^{-i\kappa \hat{x} \cdot z} ds(z) + R(\hat{x}, \hat{\eta}, \kappa) \\ &= 2(2\pi)^{m/2} \beta(\kappa) \kappa^2 (1 - \hat{\eta} \cdot \hat{x}) \widehat{\mathcal{X}}_\Omega(\kappa(\hat{x} - \hat{\eta})) + R(\hat{x}, \hat{\eta}, \kappa) \end{aligned} \quad (23)$$

where

$$R(\hat{x}, \hat{\eta}, \kappa) = 4\text{Im}(\beta(\kappa)) \int_{\partial\Omega_-} \frac{\partial u^i(z, \hat{\eta}, \kappa)}{\partial \nu(z)} e^{-i\kappa \hat{x} \cdot z} ds(z). \quad (24)$$

Rearranging terms in Eq.(23) yields

$$\left( u^\infty(\hat{x}, \hat{\eta}, \kappa) + \overline{u^\infty(-\hat{x}, -\hat{\eta}, \kappa)} \right) \frac{\tilde{g}(\kappa)}{\beta(\kappa)} \approx (1 - \hat{\eta} \cdot \hat{x}) \widehat{\mathcal{X}}_\Omega(\kappa(\hat{x} - \hat{\eta})) + \frac{\tilde{g}(\kappa)}{\beta(\kappa)} R(\hat{x}, \hat{\eta}, \kappa), \quad (25)$$

where

$$\tilde{g}(\kappa) := \frac{1}{2(2\pi)^{m/2} \kappa^2}, \quad m = 2, 3. \quad (26)$$

In  $\mathbb{R}^3$  the factor  $\beta(\kappa)$  is real (see Eq.(5)), so the term involving the integral  $R$  vanishes. In this case it is apparent from Eq.(25) that for a fixed incident direction  $\hat{\eta}$ , the far field data at wavenumber  $\kappa$ ,  $u^\infty(\hat{x}, \hat{\eta}, \kappa)$ , lies in the spatial frequency domain along a sphere of radius  $\kappa$  with center  $-\kappa\hat{\eta}/2$ . This is illustrated in Figure 2(a) for three wavenumbers and two incident field directions. Also clear from Figure 2(a) is that one requires a sufficient number of incident fields and/or wavelengths to adequately “cover” the spatial frequency domain in order to recover  $\mathcal{X}_\Omega$  by Fourier inversion. There is some redundancy, however, in the data in the case where data from all wave numbers and all incident directions is collected. This redundancy has been noted in the case of scattering from inhomogeneous media in [17]. Figure 2(a) serves as a graphical heuristic for a uniqueness theorem proven by Colton and Sleeman [6] which states that the scattering problem with Dirichlet boundary data is unique, given a finite number of incident fields depending on the wavenumber  $\kappa$  and the size of the scatterer.

We rewrite Eq.(25) in terms of the backprojection operator  $\tilde{\mathcal{A}}_{\tilde{g}}$  (see Eq.(17)) with kernel  $\tilde{g}$  (see Eq.(26)) by multiplying both sides of Eq.(25) by  $e^{i\kappa \hat{x} \cdot z}$  and integrating with respect to  $\hat{x}$  over the aperture  $\Gamma$ :

$$\left( \tilde{\mathcal{A}}_{\tilde{g}} u^\infty \right) (z, \hat{\eta}, \kappa) + \left( \tilde{\mathcal{A}}_{\tilde{g}} \tilde{u} \right) (z, \hat{\eta}, \kappa) \approx \int_{\Gamma} (1 - \hat{\eta} \cdot \hat{x}) \widehat{\mathcal{X}}_\Omega(\kappa(\hat{x} - \hat{\eta})) e^{i\kappa \hat{x} \cdot z} ds(\hat{x}) + \left( \tilde{\mathcal{A}}_{\tilde{g}} R \right) (z, \hat{\eta}, \kappa) \quad (27)$$

where  $\tilde{u}(\hat{x}, \hat{\eta}, \kappa) := \overline{u^\infty(-\hat{x}, -\hat{\eta}, \kappa)}$ . Unlike the density  $g_*$  satisfying Eq.(13), the density  $\tilde{g}$  does not depend on a domain of approximation  $\Omega_0$  or the point of approximation  $z$ . For points  $z \in \Omega^\circ$  satisfying  $\Omega \subset \Omega_0 + z$  for any  $\Omega_0$ , wherever  $\tilde{g}$  satisfies Eq.(10) for  $\epsilon > 0$  large enough, the backprojection operator  $\tilde{\mathcal{A}}_{\tilde{g}}$  applied to the far field data  $u^\infty(\hat{x}, \hat{\eta}, \kappa)$  approximates the scattered field  $u^s(z, \hat{\eta}, \kappa)$  with upper bounds on the pointwise error given by Eq.(11). Thus, the physical optics approximation yields an easily calculated density whose dependence on the wavenumber  $\kappa$  is *explicit*. This is discussed next.

### 3.3 Special case: backscattering

We finish this discussion of inverse scattering techniques by examining the special case of reconstructions by a single far field data measurement  $u^\infty(\hat{y}, \hat{\eta}, \kappa)$  for each incident field with direction  $\hat{\eta}$  and wavenumber  $\kappa$ ,  $u^i(x, \hat{\eta}, \kappa)$ . The limited aperture is a single point  $\Gamma = \{\hat{y}\}$ . For an incident field with direction  $\hat{\eta}$ , the aperture  $\{\hat{y}\} = \{-\hat{\eta}\}$  corresponds to *backscattered* data. This case illustrates the key differences between the density  $g$  calculated as the solution to Eq.(13), or some related optimization problem, and the density  $\tilde{g}$  predicted by the physical optics approximation Eq.(26). We begin with the physical optics approximation.

For simplicity, we consider only scattering in  $\mathbb{R}^3$ . Here Eq.(23) simplifies to

$$\left(u^\infty(-\hat{\eta}, \hat{\eta}, \kappa) + \overline{u^\infty(\hat{\eta}, -\hat{\eta}, \kappa)}\right) \frac{\tilde{g}(\kappa)}{\beta(\kappa)} \approx 2\widehat{\mathcal{X}_\Omega}(-2\kappa\hat{\eta}). \quad (28)$$

Note that, for fixed wavelength  $\kappa$ , the data  $u^\infty$  is collected along a sphere in the spatial frequency domain with radius  $2\kappa$  (see Figure 2(b)). This is reminiscent of the Radon transform, where the Fourier Slice Theorem [13, Theorem II.1.1] relates the the Fourier transform in polar coordinates to the Radon transform. Indeed, by this interpretation, the factor  $\tilde{g}$  is a *filter* in the standard filtered backprojection algorithm for inverting the Radon transform. This connection between scattering and generalized Radon transformation is well known. Interested readers are referred to [10] for details.

For the integrals over the aperture  $\Gamma = \{-\hat{\eta}\}$  in Eq.(27) to be meaningful in the case of backscattering (in particular Eq.(9) and all related integral operators) we interpret the density  $g$  as a *distribution*  $g(\hat{y}, z, \kappa) = \delta(\hat{y} - \hat{\eta})c(z, \kappa)$ , where  $c : \mathbb{R}^m \times \mathbb{R}_+ \rightarrow \mathbb{C}$  and  $\delta$  is the Dirac delta function. According to this interpretation, the density calculated by the physical optics approximation is given by

$$\tilde{g}(\hat{y}, \kappa) = \frac{\delta(\hat{y} - \hat{\eta})}{2(2\pi)^{m/2}\kappa^2}, \quad m = 2, 3, \quad (29)$$

independent of the point  $z \in \mathbb{R}^m$  or the approximation domain  $\Omega_a$ . By Theorem 1, however, in order to achieve the best approximation (in the  $L^2$  sense) to the scattered field  $u^s$  at the point  $z$  for a given generating approximation domain  $\Omega_0$  we seek an optimal choice for the constant  $c(z, \kappa)$  that yields the best approximation to the point source  $\Phi(x, z, \kappa)$  on  $\Omega_0 + z$  by the *backscattering* Herglotz wave operator  $\tilde{H}$  given by Eq.(7) acting on the distribution  $g(\hat{y}, z, \kappa)$ , that is,  $(\tilde{H}g(\hat{y}, z, \kappa))(x) = e^{i\kappa x \cdot \hat{\eta}}c(z, \kappa)$ . A similar argument to the proof of Proposition 2 shows that the solution to the finite-dimensional optimization problem

$$\begin{aligned} & \text{minimize } \left\| \Phi(\cdot, z, \kappa) - e^{i\kappa(\cdot)\cdot\hat{\eta}} c(z, \kappa) \right\|_{L^2(\partial\Omega_0+z)}^2 \\ & \text{over } c(z, \kappa) \in \mathbb{C}, \end{aligned} \quad (30)$$

is given by  $c_*(z, \kappa) = e^{-i\kappa z \cdot \hat{\eta}} c_*(0, \kappa)$  where  $c_*(0, \kappa)$  is the optimal solution to

$$\begin{aligned} & \text{minimize } \left\| \Phi(\cdot, 0, \kappa) - e^{i\kappa(\cdot)\cdot\hat{\eta}} c(0, \kappa) \right\|_{L^2(\partial\Omega_0)}^2 \\ & \text{over } c(0, \kappa) \in \mathbb{C}. \end{aligned} \quad (31)$$

A straight-forward calculation shows that the unique optimal solution to this problem is

$$c_*(0, \kappa) = \frac{1}{\int_{\partial\Omega_0} ds(x)} \left\langle \Phi(x, 0, \kappa), e^{i\kappa x \cdot \hat{\eta}} \right\rangle_{L^2(\partial\Omega_0)}, \quad (32)$$

with the corresponding optimal distribution given by

$$g_*(\hat{y}, z, \kappa) = \delta(\hat{y} - \hat{\eta}) e^{-i\kappa z \cdot \hat{\eta}} c_*(0, \kappa). \quad (33)$$

Note that  $\tilde{g}$  behaves as  $\kappa^{-2}$  while the behavior of  $g_*$  is on the order of  $\kappa^{\frac{1-m}{2}}$ . This is a critical difference for multifrequency data. In the next section we compare the results of reconstructions using both densities  $\tilde{g}$  and  $g_*$ .

## 4 Results

Since, for every wavenumber  $\kappa$ , the total field satisfies the Dirichlet boundary condition  $u = 0$  on  $\partial\Omega$ , we expect the sum of the modulus squared of the total field over all sampled wavenumbers to also be small in a neighborhood of the boundary. The images we construct are thus given by

$$f(z_i) = \sum_{k=1}^K \sum_{j=1}^J \left| u_*^s(z_i, \hat{\eta}_j, \kappa_k) + u^i(z_i, \hat{\eta}_j, \kappa_k) \right|^2. \quad (34)$$

at points  $z_i \in \mathcal{G}$  ( $i \in \mathbb{N}$ ), the computational grid, where  $u_*^s(z_i, \hat{\eta}_j, \kappa_k)$  is an approximation to the scattered field for each sampled direction  $\hat{\eta}_j$ , ( $j \in \mathbb{N}$ ) and each frequency  $\kappa_k$ , ( $k \in \mathbb{N}$ ).

Reconstructions using the point source method are accomplished in the following series of steps.

**Algorithm 3 (Multifrequency Point Source Method) :**

**Step 1:** (Generating density  $g_*(\hat{y}, 0, \kappa)$ ): Set up the generating approximation domain  $\Omega_0$  and, at each frequency  $\kappa_k$ , solve the minimization problem Eq.(13) for the generating density  $g_*(-\hat{y}_l, 0, \kappa_k)$  corresponding to the far field measurements  $u^\infty(\hat{y}_l, \hat{\eta}, \kappa_k)$  ( $l, k \in \mathbb{N}$ ).

**Step 2:** (Backprojection) At points  $z_i \in \mathcal{G}$  ( $i \in \mathbb{N}$ ), the computational grid, calculate the approximation to the scattered field  $u_*^s(z_i, \hat{\eta}_j, \kappa_k)$  for each direction  $\hat{\eta}_j$ , ( $j \in \mathbb{N}$ ) and each frequency  $\kappa_k$ , ( $k \in \mathbb{N}$ ).

**Step 3:** (Integration) Add the modulus squared of all approximated total fields, that is, for each  $z_i$  compute  $f(z_i)$  defined by Eq.(34).

For our simulations we use a kite-shaped sound-soft obstacle used in [3, Section 3.5]. This is shown in Figure 1(b). The parameter values for the approximation domain shown in Figure 1(a) are the following:  $R_1 = .07$ ,  $R_2 = 6$ ,  $\theta_\epsilon = 10^{-16}$ .

Reconstructions with the point source method are shown with densities  $g_*$  calculated via the exact optimization problem Eq.(13) and also using the first term of the Fourier series expansion of  $g_*$ . In each, the regularization parameter  $\alpha = 10^{-8}$  and the penalty parameter  $\tilde{\alpha} = 20$ . These reconstructions are compared to reconstructions using the physical optics density  $\tilde{g}$  (see Eq.(26)) in Step 2. of Algorithm 3, rather than  $g_*$ . The figures show reconstructions for four different regimes: I. full aperture,  $\Gamma = \mathbb{S}$ , sampled at 128 points, 1 incident field, and 16 wavenumbers evenly spaced on the interval  $[0.75, 10]$ ; II. quarter-aperture,  $\Gamma = \pi/2$ , sampled at 32 points 8 incident fields evenly spaced on the interval  $[0, 2\pi]$ , and eight wavenumbers evenly spaced on the interval  $[0.75, 10]$ ; III. limited aperture,  $\Gamma = (0, \pi/16)$  sampled at 4 points, 32 incident fields evenly spaced on the interval  $[0, 2\pi]$ , and 16 wavenumbers evenly spaced on the interval  $[0.75, 10]$ ; and IV. backscattering with 128 incident fields evenly spaced on the interval  $[0, 2\pi]$ , and 16 frequencies evenly spaced on the interval  $[.75, 10]$ . In each of the experiments above, the same number of data points is used, that is, the number of far field measurements times the number of incident fields times the number of frequencies used is always equal to 2048.

Our numerical results indicate that the critical factor for reconstructions in multifrequency settings is the frequency dependence of the filter. Our results also show that the frequency dependence encoded in filters calculated by solving Eq.(13) delivers higher quality reconstructions than those generated with filters suggested by classical, high-frequency techniques. The Fourier series expansions explored here, together with a particular generating approximation domain (Figure 1(a)) allow efficient implementations of the point source method with multifrequency data.

## Acknowledgments

This work is dedicated to Rainer Kress in honor of his 60th birthday, with deep gratitude for his support and encouragement. This work was completed while the author was a post-doctoral research assistant at the University of Göttingen.

## References

- [1] H.D. Albert and A. G. Ramm, Scattering amplitude and algorithm for solving the inverse scattering problem for a class of non-convex obstacles, *J. Math Anal. Appl.* 117 (1986) 570-597.
- [2] N. N. Bojarski, A Survey of the physical optics inverse scattering identity, *IEEE Trans. Ant. Prop.* AP-20 (1982) 980-989.
- [3] D. Colton and R. Kress, *Inverse Acoustic and Electromagnetic Scattering Theory*, 2nd Ed. (Springer-Verlag, Berlin, 1998).
- [4] D. Colton and P. Monk, A novel method for solving the inverse scattering problem for time-harmonic waves in the resonance region, *SIAM J. Appl. Math.* 45 (1985) 1039-1053.
- [5] D. Colton and P. Monk, A novel method for solving the inverse scattering problem for time-harmonic waves in the resonance region II, *SIAM J. Appl. Math.* 46 (1986) 506-523.
- [6] D. Colton and B. D. Sleeman Uniqueness theorems for the inverse problem of acoustic scattering, *IMA J. Appl. Math.* 31 (1983) 253-259.
- [7] A. Kirsch and R. Kress, A numerical method for an inverse scattering problem, in: Engl and Groetsch, eds., *Inverse Problems* (Academic Press, Orlando, 1987) 279-290.
- [8] R. Kress, Integral equation methods in inverse acoustic and electromagnetic scattering, in: D. B. Ingham and L. C. Wrobel eds., *Boundary Integral Formulations for Inverse Analysis* (Computational Mechanics Publications, South Hampton, UK, 1997) 67-92.
- [9] R. Leis, Initial-boundary value and scattering problems in mathematical physics, in: *Partial differential equations and calculus of variations*, , Lecture Notes in Math., Vol.1357, (Springer, Berlin, 1988) 23–60.
- [10] R. Lies, *Initial Boundary Value Problems in Mathematical Physics* (B.G. Teubner, Stuttgart, 1986).
- [11] D. R. Luke and R. Potthast, Image processing for limited aperture inverse acoustic obstacle scattering (submitted).

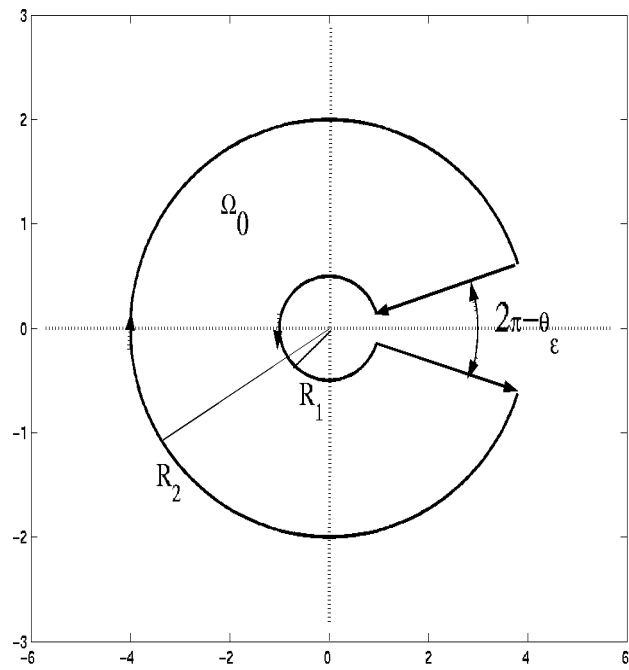
- [12] D. R. Luke and R. Potthast, The no response test – a sampling method for inverse scattering problems, *SIAM J. Appl. Math.* (to appear).
- [13] F. Natterer, *The Mathematics of Computerized Tomography* (John Wiley & Sons, New York, 1986).
- [14] R. Potthast, A fast new method to solve inverse scattering problems, *Inverse Problems* 12 (1996) 731-742 .
- [15] R. Potthast, A point-source method method for inverse acoustic and electromagnetic obstacle scattering problems, *IMA Jour. Appl. Math.* 61,(1998) 119-140.
- [16] R. Potthast, *Point Sources and Multipoles in Inverse Scattering Theory* (Chapman & Hall 2001).
- [17] A. E. Yagel, Differential and integral methods for multidimensional inverse scattering problems, *J. Math. Phys.* 27 (1986), 2584-2591.



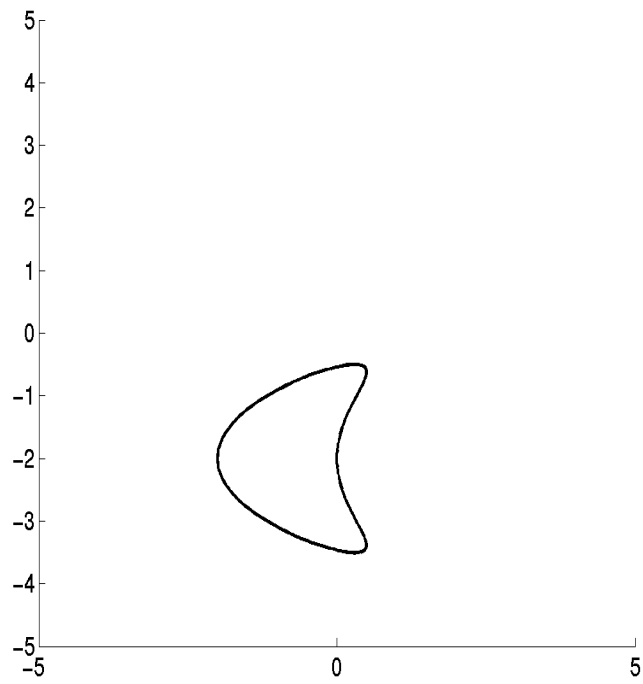
## List of Figures

- 1 (a) Domain of approximation  $\Omega_a$ . (b) Scattering obstacle  $\Omega$ . 17
- 2 Scattering data geometry for  $\mathbb{R}^2$ . (a) Full scattering data for two incident directions. (b) Backscatter only for all incident directions. 18
- 3 Plots of the values  $f(z_i)$  calculated via Eq.(34) for full aperture,  $\Gamma = \mathbb{S}$ , far field data sampled at 128 points, 1 incident field with direction  $7\pi/8$ , and 16 wavenumbers evenly spaced on the interval  $[0.75, 10]$ . (a) Reconstruction using using the physical optics density  $\tilde{g}$  (see Eq.(26)) in Step 2. of Algorithm 3, rather than  $g_*$ . (b) Reconstruction with the point source method with density  $g_*$  calculated by using the first term of the Fourier series expansion of  $g_*$ . (c) Reconstruction with the point source method with density  $g_*$  calculated by using the exact optimization problem Eq.(13). For both (b) and (c) the regularization parameter  $\alpha = 10^{-8}$ . The corresponding approximation domain is shown in Figure 1(a) with parameter values  $R_1 = .07$ ,  $R_2 = 6$ ,  $\theta_\epsilon = 10^{-16}$ . 20
- 4 Plots of the values  $f(z_i)$  calculated via Eq.(34) for quarter-aperture,  $\Gamma = \pi/2$ , 8 incident fields evenly spaced on the interval  $[0, 2\pi]$ , and 8 wavenumbers evenly spaced on the interval  $[0.75, 10]$ . (a) Reconstruction using using the physical optics density  $\tilde{g}$  (see Eq.(26)) in Step 2. of Algorithm 3, rather than  $g_*$ . (b) Reconstruction with the point source method with density  $g_*$  calculated by using the first term of the Fourier series expansion of  $g_*$ . (c) Reconstruction with the point source method with density  $g_*$  calculated by using the exact optimization problem Eq.(13). For both (b) and (c) the regularization parameter  $\alpha = 10^{-8}$  and the penalty parameter  $\tilde{\alpha} = 20$ . The corresponding approximation domain is shown in Figure 1(a) with parameter values  $R_1 = .07$ ,  $R_2 = 6$ ,  $\theta_\epsilon = 10^{-16}$ . 22

- 5 Plots of the values  $f(z_i)$  calculated via Eq.(34) for limited aperture,  $\Gamma = (0, \pi/16)$ , 32 incident fields evenly spaced on the interval  $[0, 2\pi]$ , and 16 wavenumbers evenly spaced on the interval  $[0.75, 10]$ . (a) Reconstruction using using the physical optics density  $\tilde{g}$  (see Eq.(26)) in Step 2. of Algorithm 3, rather than  $g_*$ . (b) Reconstruction with the point source method with density  $g_*$  calculated by using the first term of the Fourier series expansion of  $g_*$ . (c) Reconstruction with the point source method with density  $g_*$  calculated by using the exact optimization problem Eq.(13). For both (b) and (c) the regularization parameter  $\alpha = 10^{-8}$  and the penalty parameter  $\tilde{\alpha} = 20$ . The corresponding approximation domain is shown in Figure 1(a) with parameter values  $R_1 = .07$ ,  $R_2 = 6$ ,  $\theta_\epsilon = 10^{-16}$ . 24
- 6 Backscattering with 128 incident fields evenly spaced on the interval  $[0, 2\pi]$ , and 16 wavenumbers evenly spaced on the interval  $[.75, 10]$ . (a) Reconstruction using using the physical optics density  $\tilde{g}$  given by Eq.(29) in Step 2. of Algorithm 3, rather than  $g_*$  given by Eq.(33). (b) Reconstruction with the point source method for density  $g_*$  given by Eq.(32) and Eq.(33). 25

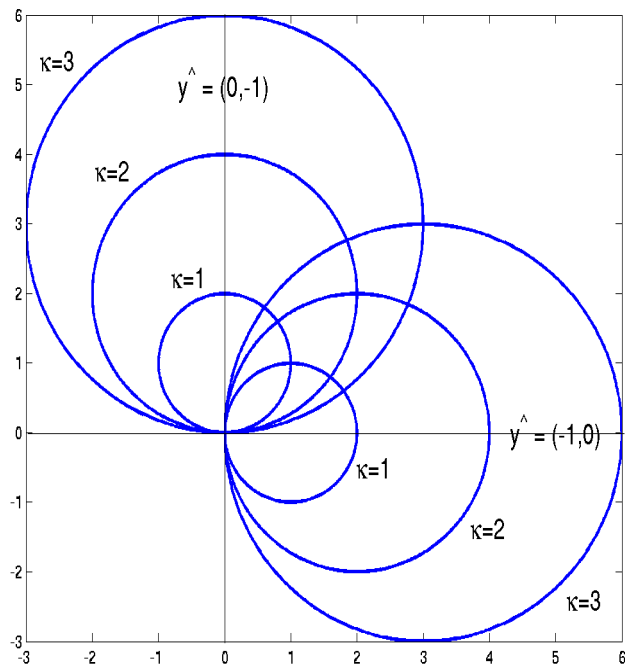


(a)

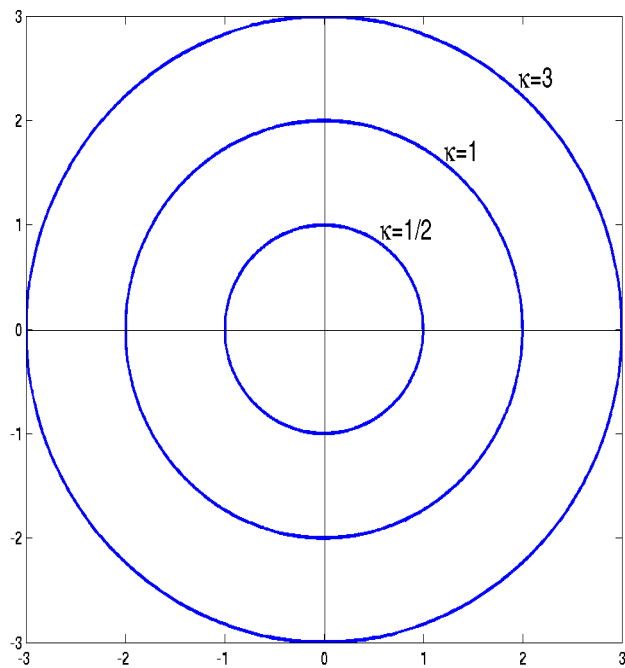


(b)

Fig. 1. (a) Domain of approximation  $\Omega_a$ . (b) Scattering obstacle  $\Omega$ .

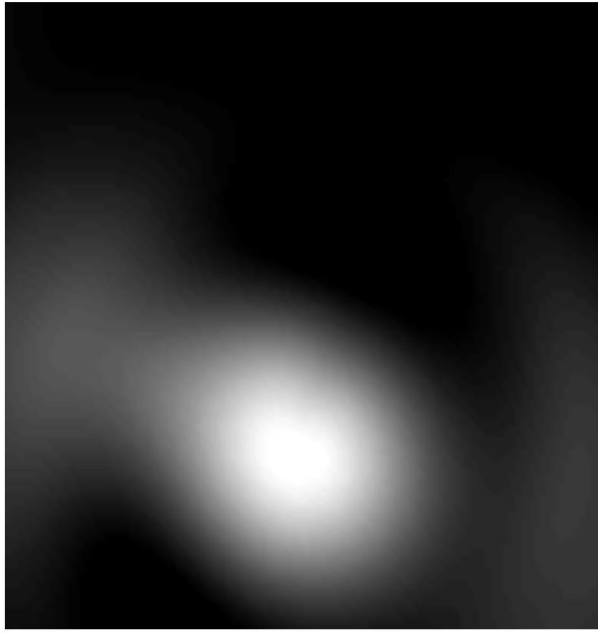


(a)

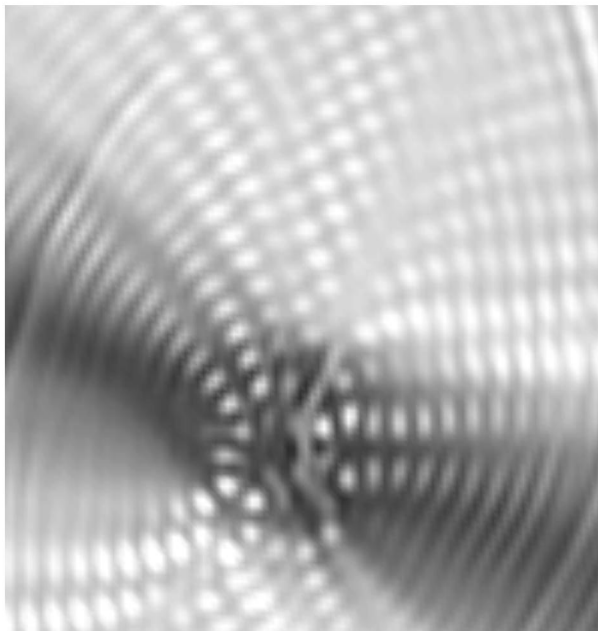


(b)

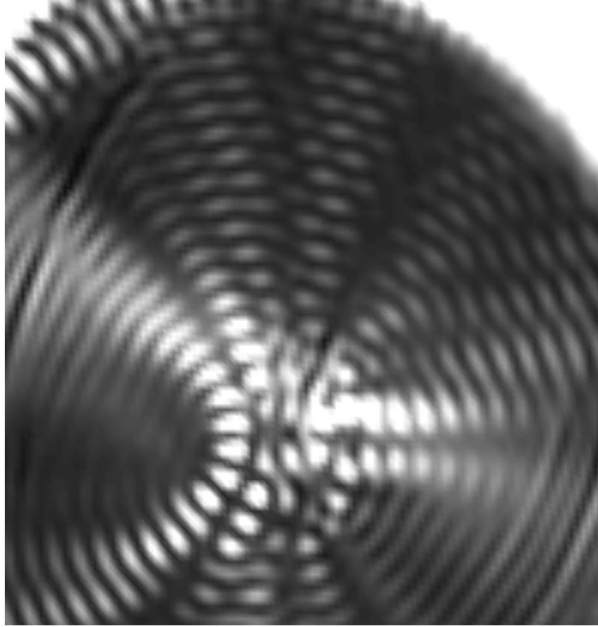
Fig. 2. Scattering data geometry for  $\mathbb{R}^2$ . (a) Full scattering data for two incident directions. (b) Backscatter only for all incident directions.



(a)

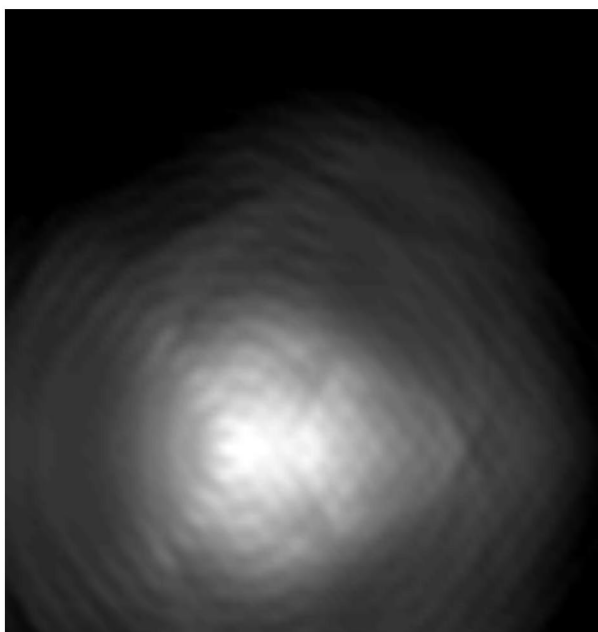


(b)

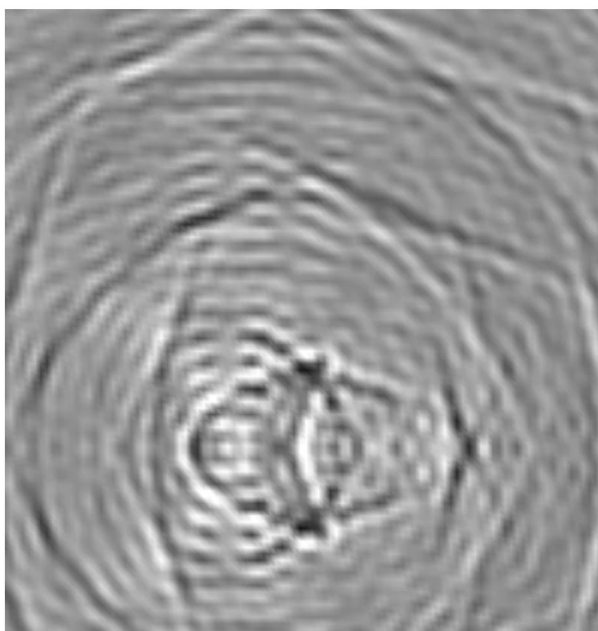


(c)

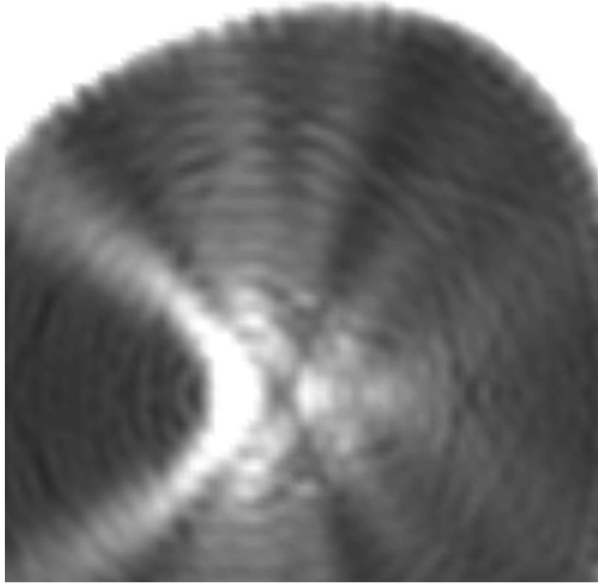
Fig. 3. Plots of the values  $f(z_i)$  calculated via Eq.(34) for full aperture,  $\Gamma = \mathbb{S}$ , far field data sampled at 128 points, 1 incident field with direction  $7\pi/8$ , and 16 wavenumbers evenly spaced on the interval  $[0.75, 10]$ . (a) Reconstruction using using the physical optics density  $\tilde{g}$  (see Eq.(26)) in Step 2. of Algorithm 3, rather than  $g_*$ . (b) Reconstruction with the point source method with density  $g_*$  calculated by using the first term of the Fourier series expansion of  $g_*$ . (c) Reconstruction with the point source method with density  $g_*$  calculated by using the exact optimization problem Eq.(13). For both (b) and (c) the regularization parameter  $\alpha = 10^{-8}$ . The corresponding approximation domain is shown in Figure 1(a) with parameter values  $R_1 = .07$ ,  $R_2 = 6$ ,  $\theta_\epsilon = 10^{-16}$ .



(a)



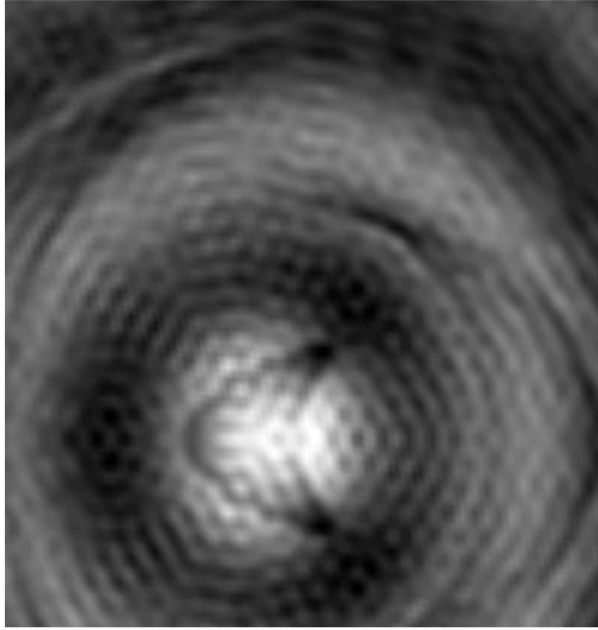
(b)



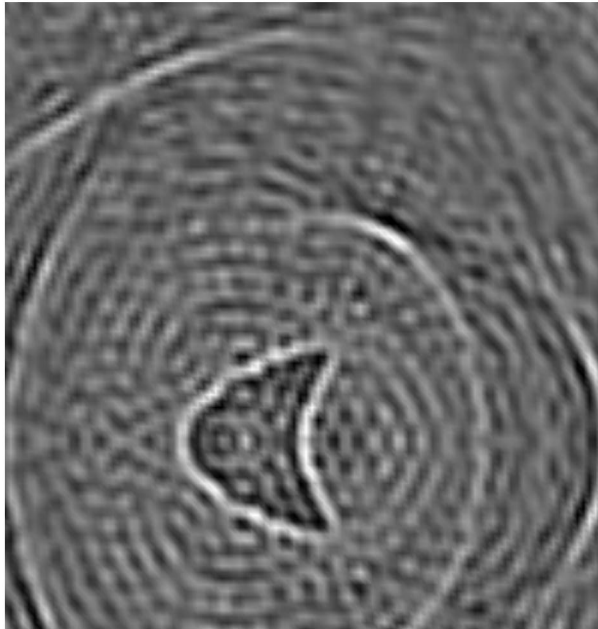
(c)

Fig. 4. Plots of the values  $f(z_i)$  calculated via Eq.(34) for quarter-aperture,  $\Gamma = \pi/2$ , 8 incident fields evenly spaced on the interval  $[0, 2\pi]$ , and 8 wavenumbers evenly spaced on the interval  $[0.75, 10]$ . (a) Reconstruction using using the physical optics density  $\tilde{g}$  (see Eq.(26)) in Step 2. of Algorithm 3, rather than  $g_*$ . (b) Reconstruction with the point source method with density  $g_*$  calculated by using the first term of the Fourier series expansion of  $g_*$ . (c) Reconstruction with the point source method with density  $g_*$  calculated by using the exact optimization problem Eq.(13). For both (b) and (c) the regularization parameter  $\alpha = 10^{-8}$  and the penalty parameter  $\tilde{\alpha} = 20$ . The corresponding approximation domain is shown in Figure 1(a) with parameter values  $R_1 = .07$ ,  $R_2 = 6$ ,  $\theta_\epsilon = 10^{-16}$ .

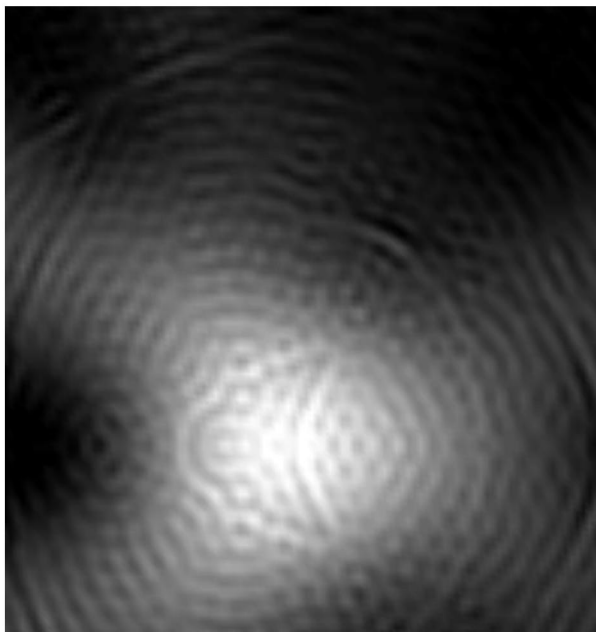




(a)

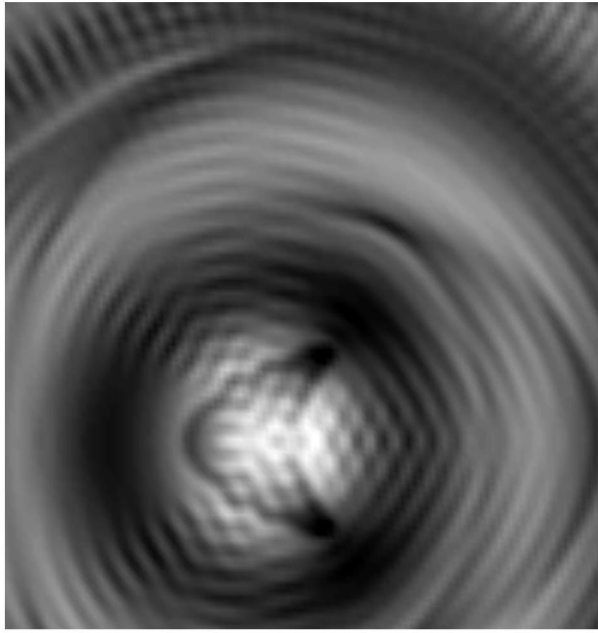


(b)

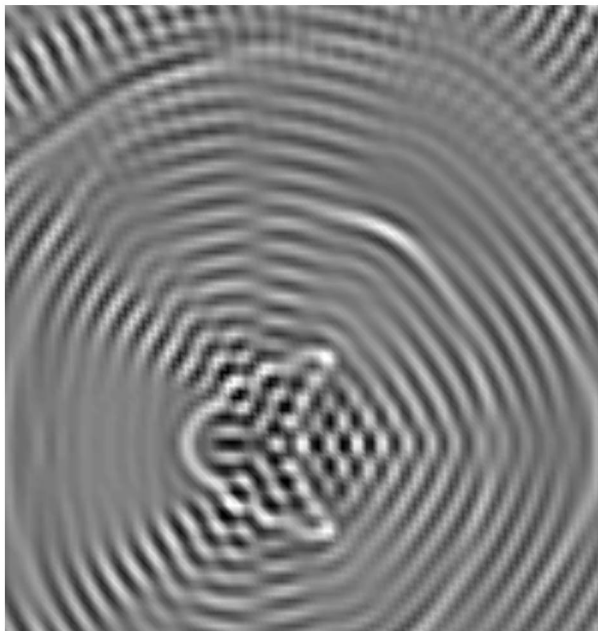


(c)

Fig. 5. Plots of the values  $f(z_i)$  calculated via Eq.(34) for limited aperture,  $\Gamma = (0, \pi/16)$ , 32 incident fields evenly spaced on the interval  $[0, 2\pi]$ , and 16 wavenumbers evenly spaced on the interval  $[0.75, 10]$ . (a) Reconstruction using using the physical optics density  $\tilde{g}$  (see Eq.(26)) in Step 2. of Algorithm 3, rather than  $g_*$ . (b) Reconstruction with the point source method with density  $g_*$  calculated by using the first term of the Fourier series expansion of  $g_*$ . (c) Reconstruction with the point source method with density  $g_*$  calculated by using the exact optimization problem Eq.(13). For both (b) and (c) the regularization parameter  $\alpha = 10^{-8}$  and the penalty parameter  $\tilde{\alpha} = 20$ . The corresponding approximation domain is shown in Figure 1(a) with parameter values  $R_1 = .07$ ,  $R_2 = 6$ ,  $\theta_\epsilon = 10^{-16}$ .



(a)



(b)

Fig. 6. Backscattering with 128 incident fields evenly spaced on the interval  $[0, 2\pi]$ , and 16 wavenumbers evenly spaced on the interval  $[\cdot75, 10]$ . (a) Reconstruction using using the physical optics density  $\tilde{g}$  given by Eq.(29) in Step 2. of Algorithm 3, rather than  $g_*$  given by Eq.(33). (b) Reconstruction with the point source method for density  $g_*$  given by Eq.(32) and Eq.(33).